Translational Line of Sight: a multi-omics longitudinal study of the murine retinal response to spaceflight hazard analogs

Prachi Kothiyal[1], Greg Eley[2], Hari Ilangovan[3], S. Robin Elgart[4], Xiao W. Mao[5], Parastou Eslami[6]

[1] SymbioSeq LLC, Ashburn, VA 20148, USA
[2] Scimentis LLC, Statham, GA 30666, USA
[3] Science Applications International Corporation (SAIC), Reston, VA 20190, USA
[4] University of Houston, Houston, TX 77204, USA
[5] Basic Sciences, Loma Linda University, Loma Linda, CA 92350, USA
[6] Universal Artificial Intelligence Inc., Boston, MA 02130, USA

Abstract

Space environment includes unique hazards like radiation and microgravity which adversely affect physiology and behavior of humans and rodent models. We assessed a multi-omics NASA GeneLab dataset where mice were hindlimb unloaded and/or gamma irradiated for 21 days followed by retinal analysis at 7 days, 1 or 4 months post-exposure.

We compared time-matched epigenomic and transcriptomic retinal profiles resulting in a total of 4,178 differentially methylated loci or regions, and 457 differentially expressed genes. Highest correlation in methylation difference was seen across different conditions at the same timepoint. Nucleotide metabolism biological processes were enriched in all groups with activation at 1 month and suppression at 7 days and 4 months. Genes and processes related to Notch and Wnt signaling showed alterations 4 months post-exposure. A total of 23 genes were differentially methylated and expressed, including genes involved in retinal disease or cataract development (*Crybb3, Fgfr1, Pitpnm3, Sipa1l3*, *Sox9*) and inflammatory response (*B4galt6, Ppm1a, Sphk1*).

This multi-omics analysis interrogates the epigenomic and transcriptomic impacts of radiation and hindlimb unloading on the retina in isolation and in combination. The results support the understanding of molecular mechanisms following spaceflight exposures and the translation of effects observed in animal models to humans.

Introduction

Spaceflight hazards such as microgravity and space radiation are anticipated to impact biological systems and could potentially affect crew health and performance both in mission and once astronauts return to Earth. These unique hazards have been thought to induce adverse changes in the central nervous system (CNS), with a frequently reported impact on ocular function [1–4]. Resources aboard space assets that have a sustained human presence like the International Space Station (ISS) are limited and it is difficult to recreate spaceflight conditions on the ground for controlled experiments. Therefore, characterization of the type and magnitude of these changes is challenging. Despite these challenges, analogs can be used to inform the understanding of

the spaceflight environment impacts on biology and support development of mitigation strategies to reduce spaceflight health risks. Ground-based analogs can also support the interrogation of biological effects from disparate stressors in isolation from one another that cannot be untangled in the spaceflight environment. Furthermore, advances in bioinformatics have expanded the potential scientific return of prior experiments provided data is accessible for re-evaluation. Fortunately, NASA's GeneLab is an open-access omics database for space-relevant biological experiments that provides access to uniformly formatted data [5].

The current study leverages transcriptomic and methylation sequencing data acquired as part of a larger experiment to understand the longitudinal effects and underlying mechanisms of low-dose radiation (IR) exposure and hindlimb unloading (HLU; an analog for microgravity) on neurovascular oxidative stress and brain function[6]. Global transcriptome profiling quantifies gene expression at the moment of sample acquisition while DNA methylation is one of the most studied epigenetic modifications involved in disease development [7–9].

Previous studies analyzed spaceflight-induced transcriptomic and epigenomic response in murine retina [10,11], or evaluated response to different ground-based hazard analogs in murine brain [6] and spleen [12]. The murine retina studies reported changes in gene expression and methylation associated with visual perception, phototransduction, and macular degeneration pathways in retinal diseases. However, these studies were performed in space where effects of both space radiation and microgravity on the retina were intertwined. In addition, these studies were performed 35-37 days after a space flight and there was no analysis done on longitudinal changes in the retina due to radiation or microgravity.

To our knowledge, the current analysis is the first multi-omics study of longitudinal changes in the murine retina due to microgravity, low-dose radiation, or combined exposure to both. We report differentially expressed genes (DEG), differentially methylated genes (DMG), and biological processes (BP) that are exclusive to, or shared across, multiple exposure conditions and post-exposure time points. We observed similar epigenetic and transcriptomic discordance in genes and pathways reported in the NASA Twins Study [13], with some changes persistent even 4 months after exposure. This study provides an insight into the retinal response to individual spaceflight hazard analogs and their interplay at

different post-exposure stages, and contributes towards a mechanistic understanding of spaceflight-induced vision impairment.

Results

Differential expression

Out of a total of 59 samples (**Supplementary Table 1**), three were excluded from expression analysis due to low RNA integrity number values or high ribosomal RNA contamination, and two were excluded from methylation analysis due to GC content bias. Principal component analysis with global transcriptomic data showed separation across post-exposure time points (**Supplementary Figure 1**). For differential gene expression and methylation analyses, each experimental group was compared against a control group (no radiation or HLU) with matched post-exposure duration, leading to a total of nine comparisons (**Table 1, Figure 1A**).

Hierarchical clustering using DEG ($|\log_2(\text{fold-change})| \geq 0.263$; adjusted p-value ≤ 0.05) across different experimental groups revealed clusters within exposed and control populations (**Figure 1B**). The highest number of DEG (275) were detected in the 7 day irradiation (IR) alone group (**Table 1, Figure 1A**). *Enrichr* [14] shows these genes to be enriched in ocular disease terms (**Supplementary Table 2**). At 7 days post-exposure, no significant disease association was detected for DEG in the HLU alone group, and no DEG were found in the HLU+IR (combination of hindlimb unloading and irradiation) group. At 1 month post-exposure, HLU+IR showed the highest number of DEG (64); *ToppGene* [15] showed enrichment for these genes in the *somatodendritic compartment* (adjusted p-value 8.24e-08; 20 genes), and included 15 genes known to be targets of *mmu-miR-466*, a miRNA that regulates age-related macular degeneration [16] (**Supplementary Table 3**). In the 1 month IR group, 7 genes were differentially expressed with > 2-fold change and adjusted p-value < 0.01 (down-regulated: *Pon1, Sult1c1, Ermn, Stra6, Tmem72, Gm24514;* up-regulated: *Bc1*). Four DEG were detected in the 4 months HLU (*Enpp2, Col5a2, Lrat, mt-Co2*) and HLU+IR (*Rgr, Rpe65, mt-Co2, Klhdc7a*) groups, whereas *Prss56* was the only DEG in the IR group.

Overlapping differentially expressed genes across exposure groups

Nine DEG were common between the HLU alone and IR alone groups at 7 days (down-regulated: *Arl2bp, Chrna6, Egln1, Map2k1, Stmn2*; up-regulated: *Ccn2, Mbd6, Sox9, St6galnac2, Zfp36l1*) (**Figure 1C**). *Bc1* and *Pgk1* were significantly up-regulated in all exposure groups at 1 month. Zinc finger protein *Zc3h11a* was significantly down-regulated in the HLU only group at 7 days but up-regulated at 1 month. *Zc3h11a* expression has been shown to be altered in the murine retina and sclera in an experimental myopia mouse model [17]. Only a single common DEG was observed between the HLU+IR and HLU groups at 4 months (*mt-Co2*; up-regulated). *mt-Co2* is located in the mitochondrial inner membrane and is an essential subunit of cytochrome c oxidase, the terminal component of the mitochondrial respiratory chain [18]. An integrated analysis of mammalian spaceflight data has reported the kidney to show an induction of *mt-Co2* [19].

Differential methylation

The 1 month HLU+IR group showed the highest total number (957) of differentially methylated loci (DML) and regions (DMR) in known genes (**Table 1, Figure 2A**). All the groups had more DML and DMR with hypermethylation than with hypomethylation. Among the hypermethylated loci, a higher proportion of methylation differences were associated with CpG shores than with islands except in all three exposures at 4 months (**Figure 2A**). Conversely, more hypomethylated loci overlapped with CpG islands than with shores in the majority of the groups except in all three groups at 7 days. The exposure groups at 4 months contained a higher proportion of total DML within CpG islands than shores compared to the other time points (**Figure 2A**). Top DML (> 20% methylation difference) within CpG islands and exclusive to 4 months post-exposure were found in 17 genes across 4m HLU (hypo: *Utp14a*; hyper: *Dlgap3*), 4m IR (hypo: *Gm7855, Rtn4rl2*; hyper: *Maz, Shank3*), and 4m HLU+IR (hypo: *Bag3*; hyper: *Aspdh, Map7d1, Map7d2, Morc4, Pcdh1, Pdzd11, Pik3ap1, Rtn4rl2, Suv39h1, Xk*).

Correlation in methylation differences across exposure groups

All methylated loci within genes and with q-value $\leq$ 0.05 were selected, and pairwise correlation between methylation differences in common sites matched by genomic coordinates were obtained for all possible pairs across the nine groups (**Figure 2B**). The highest correlation in methylation difference was seen for loci across different exposures at the same post-exposure time point. A DML

in a CpG island within *Bclaf3* promoter was hypermethylated in four groups (~15% in 1m HLU, 4m IR and 4m HLU+IR, and 26% in 1m HLU+IR), and another CpG island DML in *Tmc8* promoter was common across all three exposure groups at 7 days (10% hypermethylation). The top DML shared across all three exposures were in *Cav2* at 7 days (30% hypermethylation), *Grip2* at 1 month (20% hypermethylation), and *Sorbs2* at 4 months (8% hypermethylation).

Overlapping differentially methylated genes across exposure groups

A number of genes containing DML or DMR were observed in multiple exposure groups and post-exposure time points (**Figure 2C**). *Bcl11b, Bclaf3, Gse1, Necab2, Plec* and *Tafa5* were each differentially methylated in five out of the nine groups. Six genes (*Adamts5, Gse1, Rbm15b, Fscn2, Satb1, Tenm3*) were shared across different time points after radiation exposure, with *Adamts5* and *Fscn2* promoters being hypermethylated even after 4 months of exposure to radiation alone. The promoter region of *Pcdh19,* a protocadherin, was hypermethylated (> 20% methylation difference) at all three time points for HLU+IR and also in HLU alone at 7 days. *Bclaf3* was hypermethylated in five groups (HLU at 7 days and 1 month, HLU+IR at 1 month and 4 months, and IR and 4 months), and CpG islands in *Hmgb3* promoter were hypermethylated in HLU and HLU+IR at both, 7 days and 1 month.

Biological processes affected by spaceflight hazard analogs across multiple conditions and post-exposure time points

Shared and exclusive biological processes across exposures and time points based on differential expression

The top BP significantly enriched across all conditions 7 days after exposure included *morphogenesis of epithelium*, *ATP metabolism*, and *nucleotide metabolism* (**Figure 3A**). Processes related to *epithelial morphogenesis* were activated in the exposure groups, whereas all other processes were suppressed across the three conditions. All shared processes were activated in the 1 month groups, with the exception of *axon guidance* and *cell junction assembly*, which were suppressed in the radiation only group. Common processes in the 1 month groups were related to *amine transport*, *regulation of membrane potential*, *synaptic vesicle exocytosis*, and *neurotransmitter transport*. At 4 months post-exposure, the top processes shared across the three exposure conditions were

suppressed. These included *lens development in camera-type eye, wound healing, angiogenesis,* and *sulfur compound metabolic process*.

Processes that were significantly enriched at all post-exposure time points for a given exposure condition were evaluated (**Figure 3B**). *Nucleotide metabolism* was suppressed at 7 days and 4 months but activated at 1 month in mice subjected to microgravity alone, whereas *epithelial tube morphogenesis* and *lens development* were activated at 7 days but suppressed at all later time points, and *detection of light stimulus* was suppressed at 7 days and subsequently activated at 1 month and 4 months. *Retina homeostasis* was suppressed in the radiation only groups at 7 days and 1 month but activated at 4 months, *eye morphogenesis* was activated at 7 days and suppressed subsequently, and *synaptic vesicle endocytosis* was suppressed at 7 days but activated at all later time points. In the combination groups, *postsynapse assembly* was activated at all time points, *nucleotide metabolism* was activated only at 1 month, and *Rho signal transduction* was activated at 7 days and 1 month followed by suppression at 4 months. *Nucleotide metabolism* and related processes were significantly enriched in all nine groups with consistent activation at 1 month and suppression at 7 days and 4 months. As a complementary approach, BP exclusive to each exposure condition (enriched in $\geq$ 2 post-exposure time points), or exclusive to each post-exposure time point were also examined (**Figures 3C, 3D**).

Over-represented biological processes based on differential methylation

Over-representation analysis (ORA) was applied separately to hypo- and hypermethylated genes, and only the hypermethylated genes resulted in significantly over-represented processes (**Table 2**). ORA is conducted by iteratively counting the number of genes shared between a preselected input gene set (e.g., genes differentially methylated based on cutoffs for significance and magnitude of change) and each annotated gene set (e.g., all genes in a GO category), and applying a hypergeometric test to determine the statistical significance of the overlap [20]. Since all the groups showed differential methylation in a sizable set of genes compared to differential expression, ORA was suitable for methylation whereas gene set enrichment analysis (GSEA) was more appropriate for gene expression as it does not require an arbitrary cutoff for selecting significant genes. The 1 month HLU+IR group showed the highest number of over-represented processes, followed by 7 days HLU. Nine processes were enriched in 4 months HLU+IR and included *nervous system development*,

neurogenesis, and *neuron differentiation.* Genes with hypermethylation and involved in the regulation of these processes included oncogenes and tumor suppressors such as *Wnt3, Trp53, Plk2, Sox10, Rap1gap, Paqr3* and *Bex1.*

Integrated analysis of genes and biological processes impacted at transcriptomic and epigenomic levels

A total of 23 genes were differentially expressed and contained at least one DML or DMR at an adjusted p-value cutoff of 0.05 (**Table 3**). *Eef1a1*, a protein involved in peptide chain elongation, was down-regulated and hypomethylated in groups exposed to radiation or microgravity 7 days post-exposure. Crystallin *Crybb3* and signal-induced proliferation-associated *Sipa1l3,* both implicated in cataract, were up-regulated and hypermethylated 7 days after exposure to IR or HLU, respectively. Fibroblast growth factor 1 (*Fgfr1*) has been known to mediate photoreceptor rescue effect in response to retinal injury [21], and the gene was up-regulated and hypomethylated 7 days after radiation. *Ncor2*, a gene in the Notch signaling pathway, was up-regulated with hypermethylation in the gene body in 7 days IR. Plectin *Plec*, a cytolinker protein involved in cytoskeletal organization, was up-regulated and hypermethylated. Filamin *Flnb* was also up-regulated and hypermethylated and is known to be involved in microvascular development [22]. No common differentially expressed and methylated genes were found in any of the exposure groups at 4 months.

The BP and constituent genes shared within a given group with significant over-representation based on methylation data and enrichment in expression analysis were also obtained (**Table 4**). Only 1 month and 4 months HLU+IR groups showed shared processes. *Small GTPase mediated signal transduction* was one such process activated in the 1 month HLU+IR group. Shared genes included apoptosis associated *Aatk* (involved in neuroblastoma), beta arrestin *Arrb1 (*part of *Wnt*, *Notch*, and *Hedgehog signaling* pathways), Rho GTPase activating *Arhgap28*, ephrin *Ephb2*, which is also dysregulated in murine brain following hindlimb unloading [6], phosphatase and actin regulator *Phactr4*, and *Timp2* (involved in open angle glaucoma). *Cacna1c* was among the genes involved in *ion transport;* another calcium voltage-gated channel subunit, *Cacna2d4*, was also impacted in the murine retina after spaceflight [10].

Discussion

Spaceflight is an environment to which Earth-based biological systems have not yet adapted. Changes in gravity as well as radiation exposure that differs from terrestrial radiation both in terms of intensity and type, are the two primary naturally occurring hazards the human body contends with during space travel. It is crucial to characterize the impacts of these hazards to ensure the crew and NASA as an agency are appropriately informed. While hazards will be experienced concurrently in spaceflight, important information about the potential interactions between hazards can reveal how impacts can be appropriately mitigated. Different countermeasure strategies will need to be employed if hazards modulate similar or divergent BP.

The current study provides insights on BP related to retinal dysfunction due to radiation and microgravity alone, and concurrently, at different time points, allowing us to understand the longitudinal changes. Expression and methylation changes in the retina peaked at 7 days with exposure to HLU or IR alone, and at 1 month with HLU+IR (**Table 1**). By 4 months, the number of DEG had reduced to less than 5 in all groups while the number of DMG in HLU+IR was lower than at 1 month but still higher than 7 days. Compared to expression results from other tissue types collected in accompanying studies, spleen data from 7 days post-exposure showed highest number of DEG in HLU alone [12], brain data from 4 months had most DEGs in HLU+IR [6], whereas the retina results presented here showed most DEGs in IR alone at 7 days, and HLU+IR at 1 month. Combined stressors can induce complex responses further regulated by factors such as radiation type, post-exposure duration, and tissue type. Our analysis showed that BP related to *microtubule dynamics* were enriched exclusively in HLU alone (**Figure 3C**). IR-specific BP included *DNA conformation changes*, *Golgi organization*, *protein-DNA complex assembly*, and *type I interferon response*. Lastly, BP exclusive to HLU+IR were *postsynaptic density organization* and *regulation of AMPA receptors*. Given the conflicting results from various studies addressing synergies between microgravity and radiation and their impact on DNA damage repair and cellular repair [23], further work is needed to understand their interplay.

Each post-exposure time point was associated with distinct BP enriched across multiple conditions only at the given time point (**Figure 3D**). At 7 days, BP related to *proteasomal protein catabolism* were suppressed in all groups, and *mammary*

gland morphogenesis was activated in IR and HLU+IR. Oncogenesis in the retina and breast have been linked by the regulation of cyclin D1 [24]; the gene encoding cyclin D1, *Ccnd1*, was significantly up-regulated 7 days after exposure to IR but was not differentially expressed at the later time points. *mRNA catabolic process* (suppressed) and *ion transmembrane transport* (activated) were among the BP exclusive to 1 month post-exposure. At 4 months, *glycerolipid metabolism*, *pigmentation*, and *brown fat cell differentiation* were suppressed.

Processes related to *nucleotide metabolism* were enriched in all the groups with activation at 1 month and suppression at 7 days and 4 months for all exposures. The magnitude of normalized enrichment score (NES) was lowest at 4 months. The suppression of nucleotide metabolism has been shown to play a role in the establishment and maintenance of the stable growth arrest of oncogene-induced senescence [25]. Further work is required to understand the mechanism behind the activation at 1 month with a return to being suppressed at 4 months. *Pdk1* was within the gene set for *nucleotide metabolism* processes across all nine groups, and its expression was decreased at 7 days and 4 months but increased at 1 month in all exposure groups (**Supplementary Figure 2**). *Pdk1* is a kinase known to play a key role in regulation of glucose and fatty acid metabolism, and is involved in cellular response to hypoxia [26]. At 7 days, the HLU+IR group showed no DEG and fewer DMG compared to the HLU or IR alone groups (**Table 1**). The BP activated exclusively in IR but not enriched in HLU+IR at 7 days included *response to wounding, innate immune response, regulation of interleukin-6 production, heart morphogenesis, lipid metabolism,* and *epithelial cell proliferation* (**Supplementary Figure 3A**). The processes suppressed exclusively in IR were related to *telomere organization, DNA repair, ncRNA metabolism, detection of light stimulus,* and *organelle localization by membrane tethering* (**Supplementary Figure 3B**).

Several genes known to be implicated in ocular diseases were found to be impacted at the transcriptomic and epigenomic levels. The top DEG (> 2-fold change) in the 7 day radiation only group were *Cryaa, Cryba1, Cryba2, Cryba4, Crybb1, Crybb2, Crybb3, Crygs, Bsfp1.* ToppGene and DisGeNET [27] showed these genes to be associated with *nuclear and congenital cataracts* (**Supplementary Table 2**). However, these genes were not dysregulated 1 month or 4 months after exposure to radiation alone. *Stra6* and *Pon1* were among the top genes (> 2-fold change and adjusted p-value < 0.01) down-

regulated in the 1 month IR group. GeneCards [26] shows these genes to be associated with microphthalmia and diabetic retinopathy, respectively. *Prss56*, a gene implicated in human and murine refractive development and myopia [28], was the only DEG in the 4 months IR group. A key component of the MAP kinase signal transduction pathway, *Map2k1*, was down-regulated in the IR and HLU+IR groups at 7 days but up-regulated at 1 month. *Bc1*, a non-coding RNA known to affect vascular development [29] and structural plasticity [30] was significantly up-regulated in all three exposures at 1 month.

The gene encoding *Myc*-associated zinc-finger transcription factor, *Maz*, has been known to play a role in eye development [31] and was one of the genes exclusive to the 4 months radiation group containing a hypermethylated locus overlapping with the promoter and a known CpG island. *Adamts5* encodes a disintegrin, a protein class known to be associated with age-related macular degeneration and was dysregulated in the murine retina after spaceflight [11], and *Fscn2* has been proposed to play a role in photoreceptor disk morphogenesis. Both these genes were hypermethylated even at 4 months after radiation. *Hmgb3,* a member of the high-mobility group superfamily and a transcription factor known to be impacted by spaceflight [10], showed hypermethylation in CpG islands overlapping promoter region in the combination and HLU groups at 7 days and 1 month, but not at 4 months.

Of the DMG involved in *regulation of neurogenesis* 4 months after HLU+IR exposure (**Table 2**), the promoter region of the brain expressed X-linked gene, *Bex1*, contained 4 hypermethylated sites overlapping a CpG island. The gene has been reported to show promoter hypermethylation in malignant glioma cell line specimens [32]. Five genes (*Map7d2, Morc4, Pdzd11, Suv39h1, Xk)* in chromosome X showed > 20% hypermethylation in the promoter region overlapping known CpG islands exclusively in 4 months HLU+IR. However, no significant changes in gene or isoform expression were observed. Further work is needed to understand the significance of hypermethylation in these genes. The last exon of *Rtn4rl2* showed > 20% hypomethylation in 4 month IR and hypermethylation in 4 month HLU+IR. The gene has been predicted to be involved in cell surface receptor signaling pathway, and negative regulation of neuron projection development. *Cell junction assembly* was over-represented in 7 days HLU and 4 months HLU+IR, and *homophilic cell adhesion via plasma membrane adhesion molecules* was shared between 1 month and 4 months

HLU+IR. Five of the genes from these pathways that were hypermethylated even at 4 months are also in the *Wnt signaling pathway* (*Wnt11,* protocadherins *Pcdh1* and *Pcdh19,* cadherins *Cdh1* and *Cdh13,* and *Sdk1*).

Processes related to *Wnt signaling pathway* were significantly enriched in multiple groups, with activation in IR and HLU+IR at 7 days, and suppression in 1 month HLU, and all three exposures at 4 months. *Wnt signaling pathway* is critically involved in cell-cell communication and regulates tissue homeostasis [33,34]. Altered activities may promote tissue degeneration [35]. Wnt signaling plays a role in eye organogenesis [36] and genes in the pathway have been reported to be impacted by spaceflight [11]. The pathway has also been shown to be affected by spaceflight in 3D-cultured neural stem cells [37] and human cardiovascular progenitor cells [38]. In the 7 days IR group, several of the genes involved in Wnt signaling were also significantly differentially expressed (*Adgra2, Ccnd1, Ctnnd1, Dkk3, Egfr, Gpc4, Lrp5, Plpp3, Sox9, and Znrf3)* and were implicated in ocular diseases (**Supplementary Table 2**). *Bclaf3* has been proposed to regulate proliferation/apoptosis by suppressing Wnt signaling in the mouse gastric epithelium [39], and showed hypermethylation in the promoter within four of the groups including IR and HLU+IR at 4 months.

A total of 23 genes shared differential expression and methylation (**Table 3**). Of these, 14 had differential methylation in the promoter region and 9 in the gene body. A negative correlation between expression and methylation changes was seen in 3 and 6 genes with differential methylation in the gene body or promoter, respectively. The rest showed a positive correlation. Recent studies have expanded the understanding of effects of DNA methylation on gene expression, especially in cancers [40]. Along with the traditional methylation-induced gene silencing, there have been patterns of consistently positive or negative correlations for all CpG sites associated with specific genes. More work is needed to understand the variation in the impact of DNA methylation on expression across different tissue and cell types, genes, and the location of CpG sites. High-mobility group containing *Sox9* is known to be involved in retinogenesis [36] and was up-regulated in 7 days HLU and IR groups, and hypomethylated in 7 days HLU. *Ppm1a* has been shown to play a crucial role in the wound healing-inflammation-angiogenesis axis in mice [41], and was down-regulated and hypermethylated 7 days after radiation but not in the later time points. *Sphk1* has been recognized to play a key role in the regulation of

inflammatory responses [42]. *Sphkap*, a modulator of *Sphk1*, was up-regulated and hypermethylated in 1 month HLU+IR. The glycoprotein *B4galt6* regulates astrocyte activation during CNS inflammation [43] and was up-regulated and hypomethylated. *Sphk1* and glycoproteins *B4galt2* and *B4galt3* were also up-regulated in 7 days HLU+IR based on spleen data from the same set of mice [12]. Transcriptional co-repressor *Tle3*, involved in Wnt and Notch signaling pathways, was up-regulated and hypermethylated in 1 month HLU+IR.

The NASA Twins Study reported *Notch3* to show epigenetic discordance in spaceflight [13]. The gene was significantly up-regulated (2-fold change) only 7 days post-irradiation. *Rbx1* and *Ncor2*, also in the Notch signaling pathway, showed 33% hypermethylation in the 4 months combination group, and up-regulation and hypermethylation 7 days post-irradiation, respectively. The NASA Twins Study also reports a decrease during flight in *leucine rich alpha-2-glycoprotein 1*, a protein involved in retinal vascular pathology. We observed *Lrg1* to be down-regulated by more than 4-fold (unadjusted p-value = 0.006) in the 1 month microgravity group and significantly hypermethylated (16.8% methylation difference) in the 4 month combination group.

Among the BP shared between differential methylation and expression analysis, *collagen fibril organization* was over-represented in 4 months HLU+IR with three overlapping constituent genes. *Col5a1* encodes an alpha chain of type V collagen. The gene family forms a major component of the basement membrane of the corneal endothelium and related genes were altered in the mouse retina after spaceflight [11]. Lysyl-oxidase like *Loxl1* has been implicated in pseudoexfoliation syndrome, a major cause of glaucoma and cardiovascular complications [44], and *Comp* plays a role in vascular wall remodeling [45].

In this multi-omics analysis persistent changes after 4 months of IR and HLU alone and in the combination group (IR+HLU) were observed, which demonstrates processes exclusive to, or shared between, exposure groups. Furthermore, there were expressed genes and processes that only presented themselves at the four month time point, which may be indicative of slower response of the eye to radiation and longer time is needed to understand the long-term effect of radiation on retina. Interestingly, the processes revealed in this study are similar to those previously reported for the retina in The NASA Twins Study [13]. Hence, our study provides confidence that murine animal models

can provide translational results for retinal changes due to radiation in defining molecular mechanisms and pathways contributing to ocular diseases.

However, our study comes with limitations. First, the number of samples was limited with only a total of 59 mice. Therefore, each exposure group at each time point was limited to 3-6 mice, resulting in an underpowered study. A follow-up study with a sufficient number of animals should be conducted to confirm the observations made in this study. Second, the animals were radiated by low-dose gamma rays which do not represent space radiation. Further studies should be implemented with GCR simulations to leverage a more realistic space radiation analog. Third, a key limitation of applying bulk RNA-Seq and RRBS to a complex tissue such as the retina with ~140 cell types [46] is that the approach averages signals over heterogeneous cell types at different transcriptomic states. As a result, true perturbations in, or correlation between, expression and methylation in a small cell population can be obscured by aggregated profiles. Fourth, comparing results from this study with those of The NASA Twins Study needs to be done with caution as analysis timepoints differed between studies (the murine retinas were analyzed four months after exposure and The NASA Twins Study showed altered expression for some of the genes 6 months after spaceflight) and correlating time points across species with such different lifespans is difficult.

Overall, the results of this study support the understanding of the longitudinal molecular mechanisms in response to spaceflight exposures and the translation of effects observed in animal models to humans. Further investigation into the interplay between these mechanisms can provide potential targets for mitigation strategies to enable astronaut health and wellbeing on and off the planet.

Methods

Experimental conditions and data availability

Transcription profiling and methylation data were downloaded from NASA's GeneLab platform (genelab.nasa.gov). GeneLab dataset GLDS-203 (https://genelab-data.ndc.nasa.gov/genelab/accession/GLDS-203/) includes RRBS data to study the impact of prolonged unloading and/or low-dose radiation on mouse retina . Based on accompanying metadata, the experiment was conducted at Loma Linda University, where a total of 59 six-month-old, female

C57BL/6J mice were subjected to one of four experimental conditions: control (N=15), hindlimb unloaded (N=14), low-dose irradiated (N=15), and combination of hindlimb unloaded and low-dose irradiated (N=15) for 21 days (**Supplementary Table 1**). Gamma radiation was delivered using ^{57}Co plates at a dose rate of 0.01 cGy/hr for a total dose of 0.04Gy [47]. Sub-groups of mice from each exposure condition were then allowed a post-exposure period of 7 days, 1 month, or 4 months, following which mice were euthanized and retinas were collected and frozen. RNA and DNA libraries were constructed and used for RNA-Seq and RRBS. The resulting data was deposited to GeneLab where RNA-seq output was processed per NASA GeneLab RNA-seq pipeline [48], and RRBS results are available in the form of raw sequencing reads. Unnormalized RNA-seq counts and raw RRBS FastQ files were downloaded from version 6 of GeneLab dataset GLDS-203, and used for the current analysis.

Differential gene expression analysis

Unnormalized RNA-seq counts from GeneLab were analyzed with *DESeq2* (v1.30.1) [49]. Counts were normalized followed by differential gene expression analysis comparing each experimental group to the corresponding post-exposure time point-matched control group. Differentially expressed genes were determined using cutoffs of 0.263 and 0.05 for log2 fold-change and adjusted p-value, respectively [6,12]. R packages *ggplot2*, *ComplexHeatmap* and *pheatmap* were used for visualization and generating heatmaps.

Differential methylation analysis

Raw RRBS reads were downloaded from GeneLab and processed with nf-core/methylseq pipeline (https://github.com/nf-core/methylseq; v1.6.1 accessed on June 23rd, 2021). In short, *FastQC* (http://www.bioinformatics.babraham.ac.uk/projects/fastqc) was used for running quality checks on reads, adapter sequences were trimmed using *Trim Galore! for Cutadapt* [50] without the *--rrbs* option as recommended for NuGEN RRBS Ovation kit, NuGEN's diversity trimming script was run, and *Bismark* [51] was used for alignment and methylation call extraction. Deduplication based on overlapping coordinates was skipped as it is not recommended for RRBS [52]. Mean Phred quality score across each base position in the read was confirmed to be $\geq$ 20 (**Supplementary Figure 4**) and *MethylKit* (v1.16.1) [53] was used for detection of differentially methylated loci with a cutoff of 0.05 and 10% for q-value and magnitude of methylation difference [11], respectively. As a complementary

approach, methylation differences were also calculated over 100-bp tiling windows to obtain differentially methylated regions [53]. Sites and regions were mapped to known genes (mm10 assembly) and known CpG islands using *genomation* [54] and *GenomicRanges* [55] packages. Promoter regions were defined as 2 kbp upstream and downstream of annotated transcription start sites. Differentially methylated genes were defined as genes containing at least one DML or DMR within their promoter region or gene body.

Gene set enrichment and over-representation analyses

GSEA for gene expression and over-representation analysis for methylation were conducted using *gseGO* and *enrichGO* functions in the *ClusterProfiler* (v3.18,1) package [56], respectively. Wald test statistics from *DESeq2* differential gene expression analysis were used to rank genes for enrichment analysis. GSEA and ORA were performed against the biological process GO category. A Benjamini-Hochberg adjusted p-value cutoff of 0.05 was used for selecting enriched terms. *REVIGO* [57] was used for reducing significant biological processes to a representative non-redundant set of terms. ORA was performed separately on hypo and hypermethylated genes to obtain significantly enriched GO biological processes (adjusted p-value $\leq$ 0.05) based on differential methylation in each group.

Author contributions

S.R.E., P.K., G.E. and P.E. made substantial contributions to the conception or design of the work. P.K. and H.I. made substantial contributions to the acquisition of data from GeneLab and setting up the computational environment for the analysis. P.K. determined the analytical approach, performed bioinformatics analysis, and wrote the manuscript. H.I. reviewed the statistical methods. X.W.M., P.K., S.R.E., G.E. and P.E. interpreted the results and edited the manuscript. X.W.M. advised on the relevance of the findings to spaceflight-associated ocular pathologies. All authors have reviewed and approved the submitted version.

Acknowledgements

The authors would like to thank Dr. Brock J. Sishc and Dr. Janice Zawaski for insightful discussions and their input to the analysis plan and the interpretation of initial results, and Dr. Newton Campbell for his help with the provisioning of

computational resources. The data used in this study has been generated as part of the work supported by NASA NRA NNX13AL97G (X.W.M.) and NASA Human Research Program Grant No. 80NSSC18K0310 (X.W.M.).

References

1. Chylack, L. T. *et al.* NASA study of cataract in astronauts (NASCA). Report 1: Cross-sectional study of the relationship of exposure to space radiation and risk of lens opacity. *Radiat. Res.* **172**, 10–20 (2009).
2. Jones, J. A. *et al.* Cataract formation mechanisms and risk in aviation and space crews. *Aviat. Space Environ. Med.* **78**, A56-66 (2007).
3. Mader, T. H. *et al.* Optic disc edema, globe flattening, choroidal folds, and hyperopic shifts observed in astronauts after long-duration space flight. *Ophthalmology* **118**, 2058–2069 (2011).
4. Alperin, N. & Bagci, A. M. Spaceflight-Induced Visual Impairment and Globe Deformations in Astronauts Are Linked to Orbital Cerebrospinal Fluid Volume Increase. *Acta Neurochir. Suppl.* **126**, 215–219 (2018).
5. Berrios, D. C., Galazka, J., Grigorev, K., Gebre, S. & Costes, S. V. NASA GeneLab: interfaces for the exploration of space omics data. *Nucleic Acids Res.* **49**, D1515–D1522 (2021).
6. Overbey, E. G. *et al.* Mice Exposed to Combined Chronic Low-Dose Irradiation and Modeled Microgravity Develop Long-Term Neurological Sequelae. *Int. J. Mol. Sci.* **20**, 4094 (2019).
7. Li, F. *et al.* Expression and methylation of DNA repair genes in lens epithelium cells of age-related cataract. *Mutat. Res.* **766–767**, 31–36 (2014).
8. Liggett, T. *et al.* Methylation patterns of cell-free plasma DNA in relapsing-remitting multiple sclerosis. *J. Neurol. Sci.* **290**, 16–21 (2010).
9. de Almeida, B. P., Apolónio, J. D., Binnie, A. & Castelo-Branco, P. Roadmap of DNA

methylation in breast cancer identifies novel prognostic biomarkers. *BMC Cancer* **19**, 219 (2019).

10. Overbey, E. G. *et al.* Spaceflight influences gene expression, photoreceptor integrity, and oxidative stress-related damage in the murine retina. *Sci. Rep.* **9**, 13304 (2019).
11. Chen, Z. *et al.* Spaceflight decelerates the epigenetic clock orchestrated with a global alteration in DNA methylome and transcriptome in the mouse retina. *Precis. Clin. Med.* **4**, 93–108 (2021).
12. Paul, A. M. *et al.* Immunological and hematological outcomes following protracted low dose/low dose rate ionizing radiation and simulated microgravity. *Sci. Rep.* **11**, 11452 (2021).
13. Garrett-Bakelman, F. E. *et al.* The NASA Twins Study: A multidimensional analysis of a year-long human spaceflight. *Science* **364**, eaau8650 (2019).
14. Chen, E. Y. *et al.* Enrichr: interactive and collaborative HTML5 gene list enrichment analysis tool. *BMC Bioinformatics* **14**, 128 (2013).
15. Chen, J., Bardes, E. E., Aronow, B. J. & Jegga, A. G. ToppGene Suite for gene list enrichment analysis and candidate gene prioritization. *Nucleic Acids Res.* **37**, W305-311 (2009).
16. Olivares, A. M. *et al.* Multimodal Regulation Orchestrates Normal and Complex Disease States in the Retina. *Sci. Rep.* **7**, 690 (2017).
17. Fan, Q. *et al.* Genetic variants on chromosome 1q41 influence ocular axial length and high myopia. *PLoS Genet.* **8**, e1002753 (2012).
18. Alston, C. L., Rocha, M. C., Lax, N. Z., Turnbull, D. M. & Taylor, R. W. The genetics and pathology of mitochondrial disease. *J. Pathol.* **241**, 236–250 (2017).
19. da Silveira, W. A. *et al.* Comprehensive Multi-omics Analysis Reveals Mitochondrial Stress as a Central Biological Hub for Spaceflight Impact. *Cell* **183**, 1185-1201.e20 (2020).
20. Huang, D. W., Sherman, B. T. & Lempicki, R. A. Bioinformatics enrichment tools: paths

toward the comprehensive functional analysis of large gene lists. *Nucleic Acids Res.* **37**, 1–13 (2009).

21. Ozaki, S., Radeke, M. J. & Anderson, D. H. Rapid upregulation of fibroblast growth factor receptor 1 (flg) by rat photoreceptor cells after injury. *Invest. Ophthalmol. Vis. Sci.* **41**, 568–579 (2000).
22. Zhou, X. *et al.* Filamin B deficiency in mice results in skeletal malformations and impaired microvascular development. *Proc. Natl. Acad. Sci.* **104**, 3919–3924 (2007).
23. Moreno-Villanueva, M., Wong, M., Lu, T., Zhang, Y. & Wu, H. Interplay of space radiation and microgravity in DNA damage and DNA damage response. *Npj Microgravity* **3**, 1–8 (2017).
24. Sicinski, P. *et al.* Cyclin D1 provides a link between development and oncogenesis in the retina and breast. *Cell* **82**, 621–630 (1995).
25. Aird, K. M. *et al.* Suppression of Nucleotide Metabolism Underlies the Establishment and Maintenance of Oncogene-Induced Senescence. *Cell Rep.* **3**, 10.1016/j.celrep.2013.03.004 (2013).
26. Stelzer, G. *et al.* The GeneCards Suite: From Gene Data Mining to Disease Genome Sequence Analyses. *Curr. Protoc. Bioinforma.* **54**, 1.30.1-1.30.33 (2016).
27. Piñero, J. *et al.* DisGeNET: a comprehensive platform integrating information on human disease-associated genes and variants. *Nucleic Acids Res.* **45**, D833–D839 (2017).
28. Paylakhi, S. *et al.* Müller glia-derived PRSS56 is required to sustain ocular axial growth and prevent refractive error. *PLOS Genet.* **14**, e1007244 (2018).
29. Wang, Y.-C., Chuang, Y.-H., Shao, Q., Chen, J.-F. & Chen, S.-Y. Brain cytoplasmic RNA 1 suppresses smooth muscle differentiation and vascular development in mice. *J. Biol. Chem.* **293**, 5668–5678 (2018).
30. Chung, A., Dahan, N., Alarcon, J. M. & Fenton, A. A. Effects of regulatory BC1 RNA deletion on synaptic plasticity, learning, and memory. *Learn. Mem.* **24**, 646–649 (2017).

31. Medina-Martinez, O. *et al.* The transcription factor Maz is essential for normal eye development. *Dis. Model. Mech.* **13**, dmm044412 (2020).
32. Foltz, G. *et al.* Genome-Wide Analysis of Epigenetic Silencing Identifies BEX1 and BEX2 as Candidate Tumor Suppressor Genes in Malignant Glioma. *Cancer Res.* **66**, 6665–6674 (2006).
33. Duchartre, Y., Kim, Y.-M. & Kahn, M. The Wnt signaling pathway in cancer. *Crit. Rev. Oncol. Hematol.* **99**, 141–149 (2016).
34. Tran, F. H. & Zheng, J. J. Modulating the wnt signaling pathway with small molecules. *Protein Sci. Publ. Protein Soc.* **26**, 650–661 (2017).
35. Logan, C. Y. & Nusse, R. The Wnt signaling pathway in development and disease. *Annu. Rev. Cell Dev. Biol.* **20**, 781–810 (2004).
36. Cvekl, A. & Mitton, K. P. Epigenetic regulatory mechanisms in vertebrate eye development and disease. *Heredity* **105**, 135–151 (2010).
37. Cui, Y. *et al.* Systematic Analysis of mRNA and miRNA Expression of 3D-Cultured Neural Stem Cells (NSCs) in Spaceflight. *Front. Cell. Neurosci.* **11**, 434 (2018).
38. Camberos, V. *et al.* The Impact of Spaceflight and Microgravity on the Human Islet-1+ Cardiovascular Progenitor Cell Transcriptome. *Int. J. Mol. Sci.* **22**, 3577 (2021).
39. Murakami, K. *et al.* A genome-scale CRISPR screen reveals factors regulating Wnt-dependent renewal of mouse gastric epithelial cells. *Proc. Natl. Acad. Sci. U. S. A.* **118**, e2016806118 (2021).
40. Spainhour, J. C., Lim, H. S., Yi, S. V. & Qiu, P. Correlation Patterns Between DNA Methylation and Gene Expression in The Cancer Genome Atlas. *Cancer Inform.* **18**, 1176935119828776 (2019).
41. Dvashi, Z. *et al.* Protein phosphatase magnesium dependent 1A governs the wound healing-inflammation-angiogenesis cross talk on injury. *Am. J. Pathol.* **184**, 2936–2950 (2014).

42. Bu, Y., Wu, H., Deng, R. & Wang, Y. Therapeutic Potential of SphK1 Inhibitors Based on Abnormal Expression of SphK1 in Inflammatory Immune Related-Diseases. *Front. Pharmacol.* **12**, (2021).
43. Mayo, L. *et al.* B4GALT6 regulates astrocyte activation during CNS inflammation. *Nat. Med.* **20**, 1147–1156 (2014).
44. Pasutto, F. *et al.* Pseudoexfoliation syndrome-associated genetic variants affect transcription factor binding and alternative splicing of LOXL1. *Nat. Commun.* **8**, 15466 (2017).
45. Halper, J. & Kjaer, M. Basic components of connective tissues and extracellular matrix: elastin, fibrillin, fibulins, fibrinogen, fibronectin, laminin, tenascins and thrombospondins. *Adv. Exp. Med. Biol.* **802**, 31–47 (2014).
46. Yan, W. *et al.* Mouse Retinal Cell Atlas: Molecular Identification of over Sixty Amacrine Cell Types. *J. Neurosci.* **40**, 5177–5195 (2020).
47. Mao, X. W. *et al.* Simulated Microgravity and Low-Dose/Low-Dose-Rate Radiation Induces Oxidative Damage in the Mouse Brain. *Radiat. Res.* **185**, 647–657 (2016).
48. Overbey, E. G. *et al.* NASA GeneLab RNA-seq consensus pipeline: Standardized processing of short-read RNA-seq data. *iScience* **24**, 102361 (2021).
49. Love, M. I., Huber, W. & Anders, S. Moderated estimation of fold change and dispersion for RNA-seq data with DESeq2. *Genome Biol.* **15**, 550 (2014).
50. Martin, M. Cutadapt removes adapter sequences from high-throughput sequencing reads. *EMBnet.journal* **17**, 10–12 (2011).
51. Krueger, F. & Andrews, S. R. Bismark: a flexible aligner and methylation caller for Bisulfite-Seq applications. *Bioinforma. Oxf. Engl.* **27**, 1571–1572 (2011).
52. Wreczycka, K. *et al.* Strategies for analyzing bisulfite sequencing data. *J. Biotechnol.* **261**, 105–115 (2017).
53. Akalin, A. *et al.* methylKit: a comprehensive R package for the analysis of genome-wide

DNA methylation profiles. *Genome Biol.* **13**, R87 (2012).

54. Akalin, A., Franke, V., Vlahoviček, K., Mason, C. E. & Schübeler, D. Genomation: a toolkit to summarize, annotate and visualize genomic intervals. *Bioinforma. Oxf. Engl.* **31**, 1127–1129 (2015).
55. Lawrence, M. *et al.* Software for Computing and Annotating Genomic Ranges. *PLOS Comput. Biol.* **9**, e1003118 (2013).
56. Yu, G., Wang, L.-G., Han, Y. & He, Q.-Y. clusterProfiler: an R package for comparing biological themes among gene clusters. *Omics J. Integr. Biol.* **16**, 284–287 (2012).
57. Supek, F., Bošnjak, M., Škunca, N. & Šmuc, T. REVIGO summarizes and visualizes long lists of gene ontology terms. *PloS One* **6**, e21800 (2011).

Figures

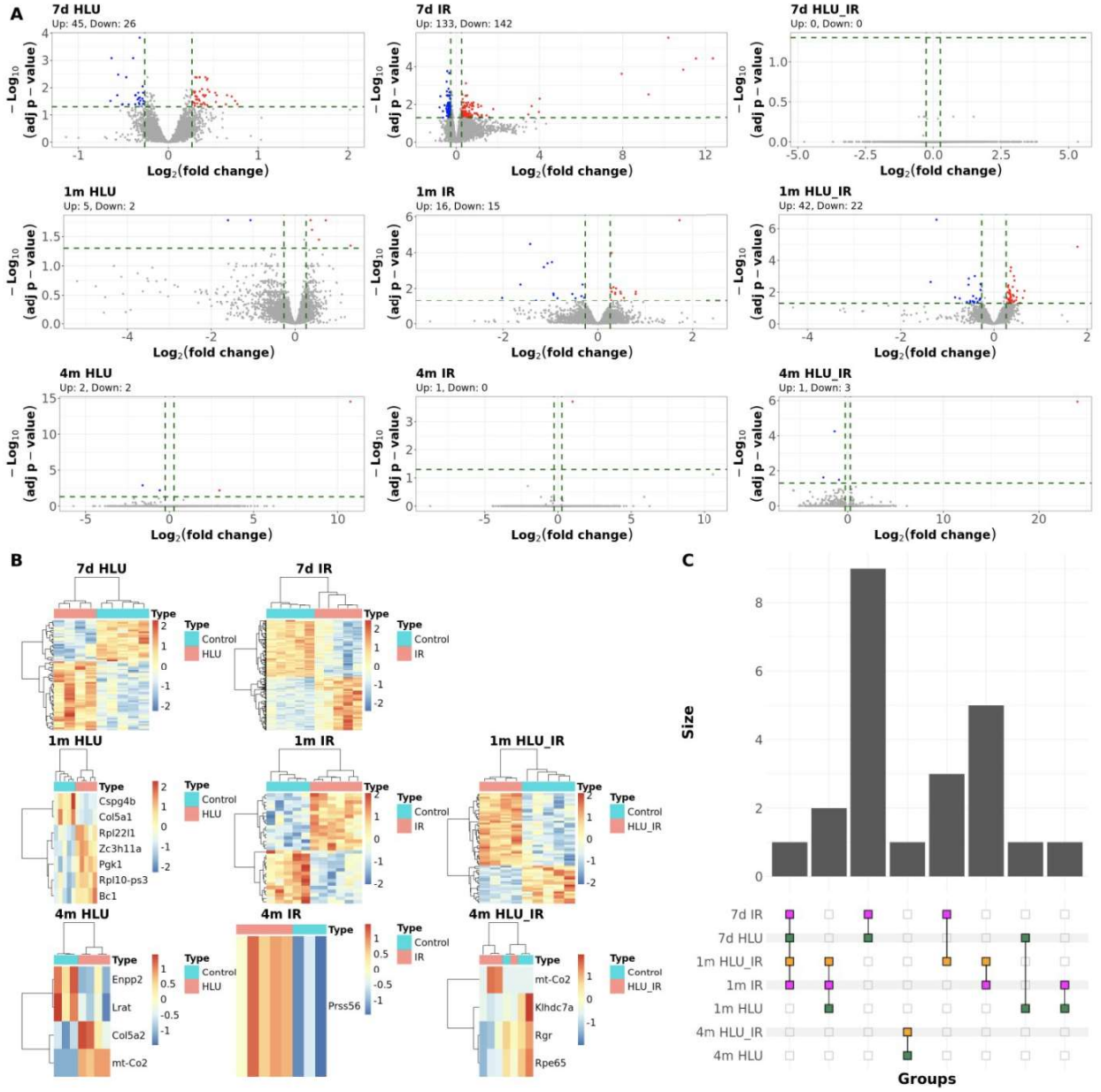

Figure 1: Differential gene expression in exposure groups. (A) Volcano plots showing DEG across each exposure condition (columns) at different time points (rows). Genes are colored by up-regulation (red) or down-regulation (blue) in exposed vs. control groups. Dashed green lines denote differential expression cutoffs of 0.05 and 0.263 for adjusted p-value and magnitude of $\log_2$(fold-change), respectively. Counts for up- and down-regulated genes in each exposure group are listed above each plot. **(B)** Heatmaps corresponding to the hierarchical clustering analysis of DEG in each group. Relative variance stabilizing transformed (VST) gene counts across samples are displayed as colors ranging from blue (low) to red (high) as shown in the key. Rows and columns are clustered using correlation distance and correspond to genes and samples, respectively. Exposure or control status are shown with colored bars at the top of each

heatmap. **(C)** Upset plot showing DEG shared between at least two of the nine groups. The Y-axis represents the number of genes in a given intersection set. The X-axis lists different intersection sets and is ordered by the number of intersecting groups in a given set. Dots are colored by exposure condition (magenta for IR, green for HLU, orange for combination). *DESeq2* was used for differential gene expression analysis and R packages *ggplot2*, *pheatmap* and *ComplexUpset* were used for visualization. *DEG* differentially expressed genes, *HLU* hindlimb unloading, *IR* irradiation.

Figure 2: Differential methylation in exposure groups. (B) Total number of differentially methylated loci and regions within genes with hyper- or hypo-methylation in each exposure group categorized by whether they overlap with known CpG islands or shores. **(A)** Pairwise correlation plots for common differentially methylated sites. Differentially methylated loci (DML) with a q-value ≤ 0.05 were selected from each of the nine groups and pairwise correlation for methylation difference was plotted for any given pair. The diagonal shows distribution of methylation difference (%) between exposure and matched control group. Pearson correlation value and significance are displayed on the right of the diagonal, and scatter plots with methylation differences for common DML from any two given groups are displayed on the left. Only significant correlations (> 3 shared DML and p-value ≤ 0.05) are displayed. **(C)** Upset plot

showing differentially methylated genes (DMG), defined as genes with their promoter or gene body containing a DML or DMR (q-value ≤ 0.05, |methylation difference| ≥ 10%), shared between at least two of the nine groups. The Y-axis represents the number of genes in a given intersection set. The X-axis lists different intersection sets and is ordered by the number of intersecting groups in a given set. Dots are colored by exposure condition (magenta for IR, green for HLU, orange for combination). R package *MethylKit* was used for differential methylation analysis, *genomation* and *GenomicRanges* were used for annotation of DML, and *ggplot2*, *ggpairs* and *ComplexUpset* were used for visualization. *DML/R/G* differentially methylated loci/region/gene, *HLU* hindlimb unloading, *IR* irradiation.

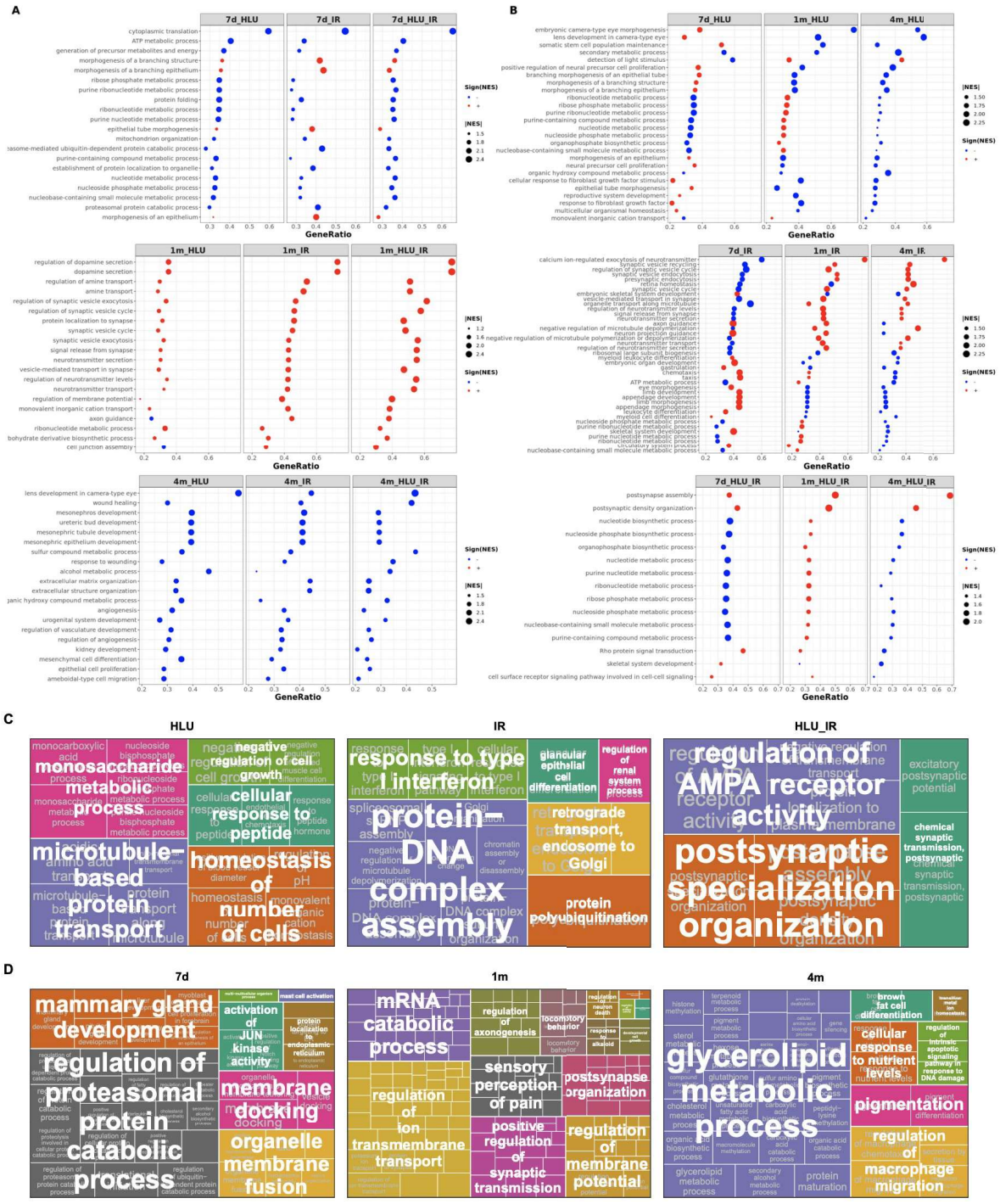

Figure 3: Common biological processes enriched in different exposure groups and at different time points. (A) Top 20 significantly enriched BP common across all exposure conditions for a given time point. **(B)** Significantly enriched BP common across all time points for a given exposure condition. Size of each point represents magnitude of normalized enrichment score (NES) while the color indicates activation (red) or suppression (blue) of the BP in the given exposure group compared to time point-matched controls. The Y-axis provides a description of common GO BP and the X-axis lists the ratio of genes that belong to a given gene set to the total number of genes in the gene set. **(C)** Non-redundant representation of BP

enriched exclusively under each exposure condition (HLU, IR, HLU+IR). **(D)** Non-redundant representation of BP enriched exclusively under each post-exposure time point (7d, 1m, 4m). *ClusterProfiler* was used for gene set enrichment analysis, the R package *ggplot2* was used for visualization, and *REVIGO* was used for reducing significant biological processes to representative non-redundant terms. *BP* biological processes, *HLU* hindlimb unloading, *IR* irradiation, *NES* normalized enrichment score.

Tables

	7 days		1 month		4 months	
	DEG	**DML/ DMR**	**DEG**	**DML/ DMR**	**DEG**	**DML/ DMR**
HLU	**71**	**743**	**7**	**716**	**4**	**134**
↓	26	173	2	67	2	55
↑	45	570	5	649	2	79
IR	**275**	**408**	**31**	**288**	**1**	**107**
↓	142	147	15	30	0	42
↑	133	261	16	258	1	65
HLU+IR	**0**	**374**	**64**	**957**	**4**	**451**
↓	0	78	22	170	3	154
↑	0	296	42	787	1	297

Table 1: Number of differentially expressed genes and differentially methylated genes across exposure groups. DEG (genes with $|\log_2(\text{fold-change})| \geq 0.263$ and adjusted p-value ≤ 0.05) and DMG (genes containing CpG loci or regions with |percent methylation difference| ≥ 10 and q-value ≤ 0.05) are listed in bold for each experimental group compared to its matched control. DEG counts are separated by down (↓) or up (↑) regulation; DML/DMR counts are separated by hypo (↓) or hyper (↑) methylation. *DEG* differentially expressed genes, *DML* differentially methylated loci, *DMR* differentially methylated regions, *HLU* hindlimb unloading, *IR* irradiation.

Group	Total number of biological processes	Top over-represented biological process (number of constituent genes)
7d HLU	22	central nervous system neuron axonogenesis (7) synapse organization (22) cell junction assembly (20) positive regulation of neuron differentiation (21) cell-cell junction organization (13) axonogenesis (21) negative regulation of blood pressure (7) myeloid cell differentiation (18) endochondral ossification (5)

		regulation of the force of heart contraction (5)
7d HLU+IR	3	regulation of nervous system process (10) telencephalon development (11) cerebral cortex development (7)
1m HLU+IR	26	positive regulation of cation transmembrane transport (15) cell-substrate adhesion (22) regulation of ion transmembrane transport (27) cellular component disassembly (23) small GTPase mediated signal transduction (25) cell-substrate junction assembly (10) positive regulation of cation channel activity (9) cellular protein complex disassembly (12) cell-matrix adhesion (15) regulation of supramolecular fiber organization (21)
4m HLU+IR	9	dendritic spine development (8) negative regulation of nervous system development (13) cell junction assembly (14) negative regulation of cell development (13) negative regulation of neurogenesis (12) homophilic cell adhesion via plasma membrane adhesion molecules (7) dendrite development (11) negative regulation of neuron differentiation (10) collagen fibril organization (5)

Table 2: Biological processes over-represented in exposure groups based on differentially methylated genes. Over-representation analysis was performed using differentially methylated genes for each group and top ten BP (or lower if there are < 10 enriched processes) are listed. Total number of BP and number of genes related to a given BP are also included. ClusterProfiler was used for over-representation analysis. *BP* biological process, *HLU* hindlimb unloading, *IR* irradiation.

Group	**Gene**	**Up or down regulated/ Hyper or hypo methylated**	**Differential methylation genomic context** (gene body vs. promoter)
7d HLU	*Cdk14* (cyclin dependant kinase) *Eef1a1* (eukaryotic translation elongation factor) *Fam222a* (aggregatin) *Pitpnm3* (membrane-associated phosphatidylinositol transfer domain-containing) *Sipa1l3* (signal induced proliferation associated) *Sox9* (SRY-box transcription factor)	Down/Hyper Down/Hypo Up/Hypo Up/Hyper Up/Hyper Up/Hypo	Promoter Promoter Gene body Promoter Gene body Gene body
7d IR	*BC031181* (cDNA sequence) *Crybb3* (crystallin) *Dcp1b* (decapping mRNA) *Eef1a1* (eukaryotic translation elongation factor) *Fgfr1* (fibroblast growth factor receptor) *Flnb* (filamin) *Mbd6* (methyl-CpG binding domain) *Ncor2* (nuclear receptor corepressor) *Plec* (plectin)	Down/Hyper Up/Hyper Up/Hypo Down/Hypo Up/Hypo Up/Hyper Up/Hyper Up/Hyper Up/Hyper	Promoter Promoter Gene body Promoter Promoter Gene body Promoter Gene body Gene body

	Ppm1a (protein phosphatase)	Down/Hyper	Promoter
1m HLU+IR	*B4galt6* (membrane-bound glycoprotein) *Kcnip3 (*potassium voltage-gated channel interacting) *Lamp5* (lysosomal associated membrane protein) *Nacad* (NAC alpha domain containing) *Rundc3a (*RUN domain containing) *Sphkap (*SPHK1 interactor, AKAP domain containing) *Tle3* (transcriptional co-repressor)	Up/Hypo Up/Hypo Up/Hyper Up/Hyper Up/Hyper Up/Hyper Up/Hyper	Promoter Promoter Promoter Gene body Promoter Promoter Gene body

Table 3: Genes with differential expression and methylation. Genes that are differentially expressed in a given group and also contain at least one differentially methylated locus or region are listed. Direction of gene regulation (up/down), methylation status (hyper/hypo), and location of DML or DMR within gene context (promoter vs. gene body) are also included. *HLU* hindlimb unloading, *IR* irradiation, *DML* differentially methylated locus, *DMR* differentially methylated region.

Group	Biological process	Overlapping genes
1m_HLU_IR	cellular protein complex disassembly	*Dmtn, Eml4, Nsf, Synj1*
	homophilic cell adhesion via plasma membrane adhesion molecules	*Celsr2, Pcdh19, Tenm3, Vstm2l*
	positive regulation of cation channel activity	*Ephb2, Kcnc2, Nedd4l*
	positive regulation of ion transport	*Akt1, Cacna1c, Cemip, Ephb2, Kcnc2, Nedd4l*
	regulation of cation channel activity	*Ephb2, Kcnc2, Nrxn1*
	regulation of ion transmembrane transport	*Akt1, Cacna1c, Cemip, Ephb2, Hcn3, Kcnc2, Kcnh1, Nrxn1*
	regulation of supramolecular fiber organization	*Chadl, Dmtn, Eml4*
	small GTPase mediated signal transduction	*Aatk, Arhgap28, Arrb1, Bcr, Cyth4, Dgki, Ephb2, Phactr4, Timp2*
4m_HLU_IR	collagen fibril organization	*Col5a1, Comp, Loxl1*

Table 4: **GO biological processes and related genes common between RNA-Seq and methylation**. BP enriched in a given group based on both, differential expression and differential methylation, are listed. Constituent genes that overlap for a given BP are included. *BP* biological process, *HLU* hindlimb unloading, *IR* irradiation

Supplementary Data

	7 days	1 month	4 months
Control	6	5	4
HLU	5	5	5

IR	4	6	5
HLU + IR	6	4	4

Supplementary Table 1: Sample counts across different exposure groups.

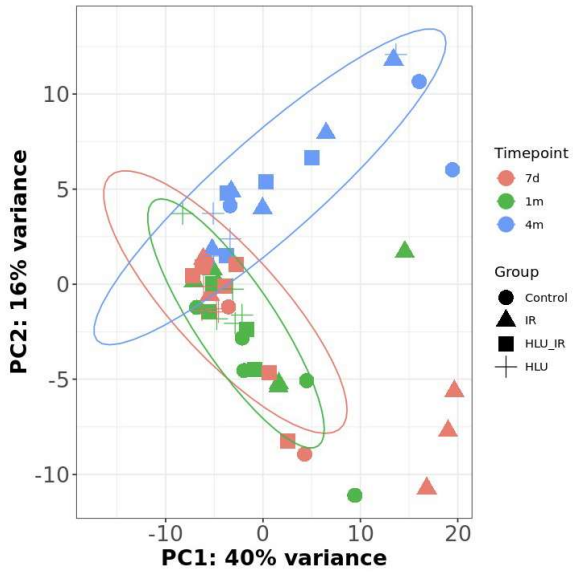

Supplementary Figure 1: PCA plot for all samples using global transcriptomic data.

Term	p-value	q-value	Genes
Cataract	2.49e-17	1.03e-13	[PRCD, GSTP1, LRP5, GUCA1B, CRYBA1, CRYBA4, EGFR, ADAMTS10, RS1, RHO, CNGA1, FLNB, PDE6A, PROM1, IMPG2, CRYGS, PDE6G, CRYBB1, ABCA4, ROM1, FN1, CRYBB3, CRYBB2, TDRD7, PEX13, DKK3, COL2A1, BFSP1, ARL2BP, RBP3, PRPH2, COL4A1, CDHR1, PXDN, ADAM9, CPE, CRYAA, KIZ]
Conductive hearing loss	6.37e-15	1.16e-11	[NOTCH3, NFIX, IQSEC2, PDE6G, PRCD, CTNND1, ABCA4, ROM1, GUCA1B, LRP5, COL2A1, ARL2BP, RBP3, PRPH2, CDHR1, CNGA1, RHO, FLNB, PDE6A, PROM1, KIZ, IMPG2]
Difficulties with night vision	8.49e-15	1.16e-11	[SLC24A1, ELOVL4, PDE6G, ABCA4, ROM1, PEX13, RIMS1, RBP3, PRPH2, CDHR1, CNGA1, RHO, ADAM9, UNC119, GNAT1, PDE6A, RAB28, PROM1, IMPG2]
Night Blindness	2.04e-14	2.10e-11	[SLC24A1, ELOVL4, PDE6G, ABCA4, ROM1, PEX13, RIMS1, RBP3, PRPH2, CDHR1, CNGA1, RHO, ADAM9, UNC119, GNAT1, PDE6A, RAB28, PROM1, IMPG2]

Glaucoma	7.18e-14	5.92e-11	[TFRC, PRCD, GSTP1, GUCA1B, XIAP, ADAMTS10, RS1, VTN, RHO, CNGA1, PDE6A, PROM1, IMPG2, PDE6G, ABCA4, ROM1, FN1, TDRD7, PEX13, PLEKHA7, VEGFA, COL2A1, ARL2BP, RBP3, PRPH2, COL4A1, CDHR1, CRYAA, KIZ]
Congenital anomaly of testis	1.19e-13	6.85e-11	[PDE6G, PRCD, ROM1, ABCA4, GUCA1B, ARL2BP, RBP3, PRPH2, CDHR1, CNGA1, RHO, PDE6A, PROM1, KIZ, IMPG2]
Progressive night blindness	1.19e-13	6.85e-11	[PDE6G, PRCD, ROM1, ABCA4, GUCA1B, ARL2BP, RBP3, PRPH2, CDHR1, CNGA1, RHO, PDE6A, PROM1, KIZ, IMPG2]
Retinal pigment epithelial abnormality	1.49e-13	6.85e-11	[PDE6G, PRCD, ABCA4, ROM1, GUCA1B, PEX13, RIMS1, ARL2BP, RBP3, PRPH2, CDHR1, CNGA1, RHO, ADAM9, UNC119, PDE6A, RAB28, PROM1, KIZ, IMPG2]
Abnormality of retinal pigmentation	1.49e-13	6.85e-11	[PDE6G, PRCD, ABCA4, ROM1, GUCA1B, PEX13, RIMS1, ARL2BP, RBP3, PRPH2, CDHR1, CNGA1, RHO, ADAM9, UNC119, PDE6A, RAB28, PROM1, KIZ, IMPG2]
Lens Opacities	1.85e-13	7.64e-11	[PRCD, LRP5, GUCA1B, CRYBA4, ADAMTS10, RS1, RHO, CNGA1, FLNB, PDE6A, PROM1, IMPG2, CRYGS, PDE6G, CRYBB1, ABCA4, ROM1, CRYBB2, TDRD7, PEX13, COL2A1, ARL2BP, RBP3, PRPH2, CDHR1, CRYAA, KIZ]

Supplementary Table 2: Disease term enrichment from Enrichr for differentially expressed genes 7 days after exposure to radiation alone.

Gene	Description	Enrichment
ATCAY	ATCAY kinesin light chain interacting caytaxin	SC
B4GALT6	beta-1,4-galactosyltransferase 6	miR-466
BNIP3	BCL2 interacting protein 3	SC
C1orf21	chromosome 1 open reading frame 21	miR-466
CACNG2	calcium voltage-gated channel auxiliary subunit gamma 2	SC
CALB1	calbindin 1	miR-466, SC
CDC42EP4	CDC42 effector protein 4	miR-466
DBN1	drebrin 1	SC
DNAI4	dynein axonemal intermediate chain 4	miR-466
ELAVL3	ELAV like RNA binding protein 3	miR-466
ELAVL4	ELAV like RNA binding protein 4	miR-466, SC
FUS	FUS RNA binding protein	SC
GABRA1	gamma-aminobutyric acid type A receptor subunit alpha1	SC
GABRA2	gamma-aminobutyric acid type A receptor subunit alpha2	miR-466, SC
GFRA2	GDNF family receptor alpha 2	miR-466
HCN4	hyperpolarization activated cyclic nucleotide gated potassium channel 4	SC
KCNAB1	potassium voltage-gated channel subfamily A regulatory beta	SC

	subunit 1	
KCNIP3	potassium voltage-gated channel interacting protein 3	miR-466, SC
LAMP5	lysosomal associated membrane protein family member 5	SC
MAP2K1	mitogen-activated protein kinase kinase 1	SC
MAPT	microtubule associated protein tau	SC
MARCHF1	membrane associated ring-CH-type finger 1	miR-466
NEURL1	neuralized E3 ubiquitin protein ligase 1	SC
NSUN3	NOP2/Sun RNA methyltransferase 3	miR-466
PDE1B	phosphodiesterase 1B	SC
PRKAR1B	protein kinase cAMP-dependent type I regulatory subunit beta	SC
PRXL2A	peroxiredoxin like 2A	miR-466
SLC2A3	solute carrier family 2 member 3	SC
SLC6A6	solute carrier family 6 member 6	miR-466, SC
UVSSA	UV stimulated scaffold protein A	miR-466

Supplementary Table 3: List of genes enriched in somatodendritic compartment (SC) and/or known to be miR-466 targets. Enrichment analysis was performed with ToppGene.

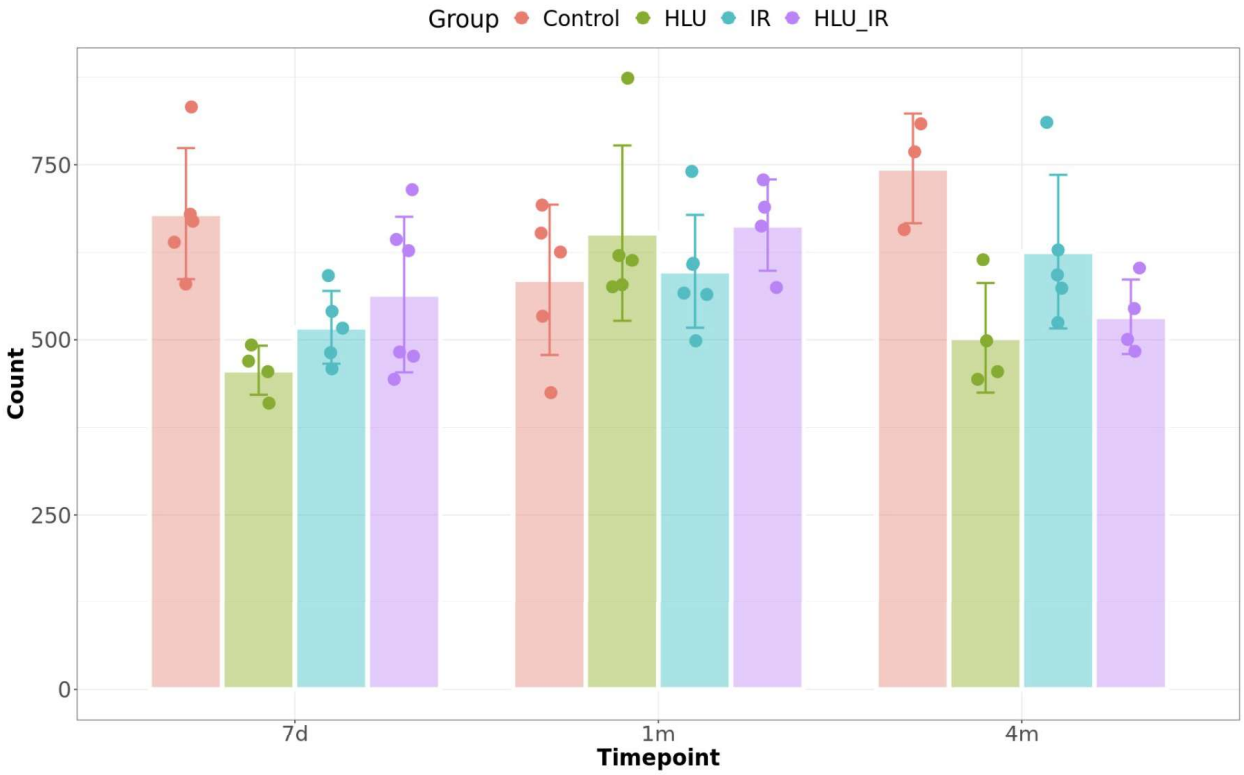

Supplementary Figure 2: Normalized RNA-seq counts for *Pdk1* across control and exposure groups at different time points.

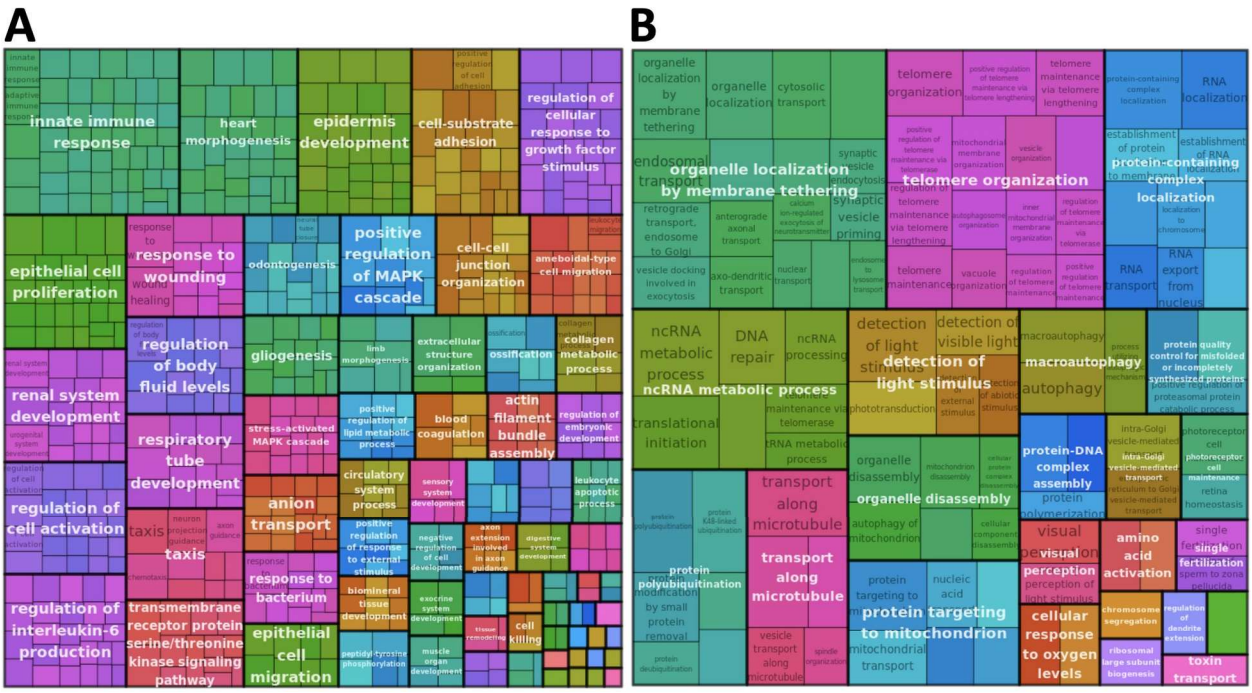

Supplementary Figure 3: GO biological processes enriched in IR but not in HLU+IR at 7 days. REVIGO non-redundant representative subset of biological processes (**A**) activated (NES > 0) or (**B**) suppressed (NES < 0) in IR but not enriched in HLU+IR. NES was calculated with ClusterProfiler GSEA. *NES* normalized enrichment score, *HLU* hindlimb unloading, *IR* irradiation.

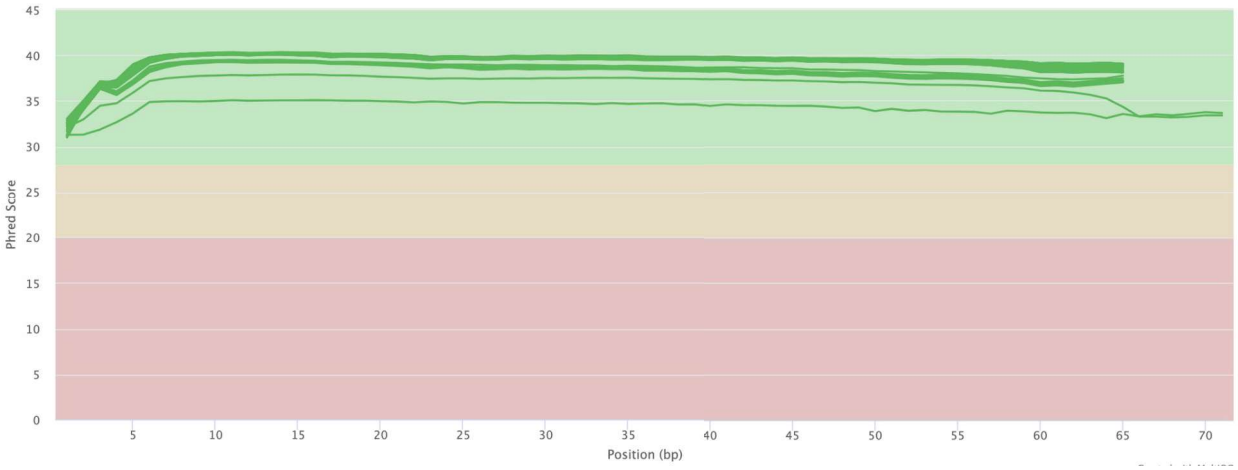

Supplementary Figure 4: Mean Phred quality score across each base position in the read.